CaV2O6: A highly effective sintering aid for 0.61CaTiO3-0.39LaAlO3 ceramics

Zizu Chen
China Jiliang University
Han Yang (young-handsome@live.com)
China Jiliang University https://orcid.org/0000-0003-2210-7880
Rongdi Guo
China Jiliang University
Guohua Wu
China Jiliang University
Yang Qiu
China Jiliang University
Mingmin Zhu
China Jiliang University
Guoliang Yu
China Jiliang University
Haomiao Zhou
China Jiliang University

Research Article

Keywords: 0.61CaTiO3-0.39LaAlO3 ceramics, sintering temperature, solid solution, crystal structure, microwave dielectric properties

Posted Date: May 17th, 2021

DOI: https://doi.org/10.21203/rs.3.rs-520206/v1

CaV_2O_6: A highly effective sintering aid for $0.61CaTiO_3$-$0.39LaAlO_3$ ceramics

Zizu CHEN, Han YANG*, Rongdi GUO, Guohua WU, Yang QIU, Mingmin ZHU, Guoliang YU, Haomiao ZHOU

Key Laboratory of Electromagnetic Wave Information Technology and Metrology of Zhejiang Province, College of Information Engineering, China Jiliang University, Hangzhou 310018, China.

Abstract:

The $0.61CaTiO_3$-$0.39LaAlO_3$ (CTLA) ceramics are widely used in relay station, aerospace and radar systems for their superior properties: remarkable quality factor and excellent thermal stability. However, some deficiencies remain, such as low permittivity and excessively high sintering temperature, which limit their development in microwave communication. Herein, we introduce CaV_2O_6 to the CTLA ceramics to solve these problems and systematically investigate its effects on sintering temperature, phase constitution, microstructure and microwave dielectric properties. The CTLA ceramics added with 0−2.0 wt% CaV_2O_6 were prepared by the traditional solid-state reaction procedure. The XRD patterns indicated that the pure phase $Ca_{0.61}La_{0.39}Al_{0.39}Ti_{0.61}O_3$ (PDF #52-1773) was obtained from all samples, which revealed that the CaV_2O_6 was dissolved into CTLA lattice to form a solid solution. As the CaV_2O_6 content increased, the strongest X-ray diffraction peaks gradually shifted toward low angles, which manifested the increase of cell volume of the solid solution. When the additive amount was 1.0 wt%, the CaV_2O_6 could high-effectively lower the sintering temperature from 1450 ℃ to 1290 ℃ and obviously promote the growth of grains. Meanwhile, the ε_r slightly increased, the $Q\times f$ significantly improved and the τ_f favorably decreased to closer to zero, then the prominent microwave dielectric performance was exhibited, with ε_r = 40.6, $Q\times f$ = 48,800 GHz (at 4.5 GHz), and τ_f = 0.78 ppm/℃. Such CTLA ceramics are expected to promote the development of high-performance and temperature-stable microwave components.

Keywords: $0.61CaTiO_3$-$0.39LaAlO_3$ ceramics; sintering temperature; solid solution; crystal structure; microwave dielectric properties

*Corresponding author: yanghan@cjlu.edu.cn (Han Yang ORCID 0000-0003-2210-7880)

1. Introduction

With the rapid development of wireless communication technologies such as millimeter-wave communication, internet of things (IoT), smart cities, self-driving cars, the low-delay, high-quality, high-integration and temperature-stable microwave components such as antenna, diplexers, filters and dielectric resonators (DRs) are increasingly the key to their applications. Due to the advantages of miniaturization, low loss, high stability and simple fabrication, microwave dielectric ceramics (MWDCs) are widely used as the pivotal resonant materials to achieve information functions in these components, and finally determine their qualities and sizes[1-3]. Therefore, high-performance MWDCs materials are becoming increasingly important [4-6].

MWDCs have many systems but the perovskite-structured (1-x)$MTiO_3$-$xNAlO_3$ (M = Sr, Ca; N = La, Nd, Sm) system has attracted great research attention due to its excellent microwave dielectric properties [7-11]. Moon et al. [12] developed the $0.65CaTiO_3$-$0.35LaAlO_3$ ceramics with remarkable performance of ε_r = 37, $Q\times f$ = 47,000 GHz, τ_f = −5 ppm/℃. Additionally, Suvorov et al. [13] obtained the (1-x)$CaTiO_3$-$xLaAlO_3$ (x = 0.3) ceramics at 1450 ℃ with permittivity of 44, quality factor of 30,000 GHz and temperature coefficient of resonance frequency of −3 ppm/℃. Jiang et al. [14] designed four different ways of preparing the $0.675CaTiO_3$-$0.325LaAlO_3$ ceramics, and prominent dielectric performance with ε_r = 45, $Q\times f$ = 37,000 GHz, and τ_f = 5 ppm/℃ was obtained at 1380 ℃. Furthermore, Tang et al. [15] introduced H_3BO_3 to the $CaTiO_3$-$LaAlO_3$ ceramics, which not only reduced the sintering temperature to 1340 ℃ but also slightly improved the performance to $\varepsilon_r \approx 40$, $Q\times f \approx$ 48,000 GHz, and $\tau_f \approx -1$ ppm/℃. Moreover, Weng et al. [16] conducted a modification study on the $CaTiO_3$-$LaAlO_3$ ceramics. Doping of 0.5 wt% B_2O_3 and 0.5 wt% CuO could reduce the high sintering temperature from 1600 ℃ to 1300 ℃, and obtained the performance of ε_r = 21, $Q\times f$ = 22,500 GHz, and τ_f = −3 ppm/℃. But in above studies, problems of excessively high sintering temperatures or dissatisfactory microwave dielectric properties exist. To further reduce the sintering temperature of $0.61CaTiO_3$-$0.39LaAlO_3$ (CTLA) ceramics and investigate the potential to modify their microwave dielectric properties, we explore a new sintering aid in this study.

Previous researches have revealed that ZnO, Bi_2O_3, CuO, MgO, La_2O_3, B_2O_3, V_2O_5, etc.

are excellent sintering aids for different ceramics [17, 18]. Additionally, in recent years, several new low-fired ceramics, such as vanadates like $Ca_5Zn_4(VO_4)_6$, $Mg_3(VO_4)_2$ and $Sr_2V_2O_7$ have been studied [19]. Among them, the CaV_2O_6 ceramics prepared at 670 °C by Yao et al. [20] presented superior performance of $\varepsilon_r \approx 10$, $Q \times f \approx 123{,}000$ GHz and $\tau_f \approx -63$ ppm/°C. Considering that the radius limit percentage (ΔR) and the electronegativity criterion (ΔS) of V^{5+} in CaV_2O_6 versus Ti^{4+} and Al^{3+} in CTLA satisfy the conditions of ion substitution and forming a solid solution [21-23], hence, in this study, we chose CaV_2O_6 as a sintering aid for CTLA ceramics and studied its effects on the sintering behavior, crystal structure and microwave dielectric performance.

2. Experimental procedure

The $0.61CaTiO_3$-$0.39LaAlO_3$ ceramics added with CaV_2O_6 were prepared via the traditional solid-state reaction route. Firstly, the high-purity La_2O_3 (≥99.90%), TiO_2 (≥99.90%) and $CaCO_3$ (≥99.90%) were stoichiometrically poured into a nylon tank filled with ethanol and zirconia balls, and ground for 6 h using a planetary ball mill. Secondly, the dried mixture was pre-fired at 1050 ℃ for 10 h. Subsequently, the calcined powders were added with 0–2.0 wt% CaV_2O_6, secondary ground, dried, secondary pre-fired and then added with 6.0 wt% polyvinyl alcohol (PVA). Later, the powders were pressed into cylindrical green bulks with the radius and thickness both in 7.5 mm under the pressure of 25 MPa. Ultimately, the green bulks were sintered into samples at 1170–1480 ℃ with the conventional heating rate of 5 ℃/min.

According to Archimedes method, the bulk density could be directly obtained using a densitometer (GF-300D, A&D Company Limited, Japan). The relative density was calculated as:

$$\rho_{relative} = \frac{\rho_{bulk}}{\rho_{theory}} \tag{1}$$

where ρ_{bulk} and ρ_{theory} are the bulk density and theoretical density, respectively. The theoretical density ρ_{theory} was calculated as:

$$\rho_{theory} = \frac{Z \times W_m}{N_A \times V_{cell}} \tag{2}$$

where Z, W_m, N_A and V_{cell} are the number of atoms associated with each unit cell, atomic weight, Avogadro constant and unit cell volume, respectively. According to the Goldschmidt rule, the

radius limit percentage (ΔR) was as follows:

$$\Delta R = \frac{|R_A - R_B|}{R_B}(\%) \tag{3}$$

where R_A and R_B are the radii of ions A and B, respectively. Substitution between ions A and B is usually favorable when $\Delta R < 15\%$ [24]. In addition, the electronegativity criterion (ΔS) proposed by Ringwood was as follows:

$$\Delta S = |S_A - S_B| \tag{4}$$

Where S_A and S_B are the electronegativities of ions A and B, respectively. When $\Delta S < 0.1$, the potential for ion substitution exists [25].

The phase constitution was investigated using X-ray diffraction (XRD) (Philips, X'pert Pro MPD, Holland). The microtopography was obtained by scanning electron microscopy (SEM) (Zeiss, MERLIN Compact, Germany). The microwave dielectric performance were studied by the Hakki-Coleman method using a network analyzer (Agilent Technologies, E5071C, USA). The temperature coefficient of the resonance frequency (τ_f) was calculated as:

$$\tau_f = \frac{(f_A - f_B)}{f_B \times 60} \times 10^6 (ppm/℃) \tag{5}$$

where f_A and f_B are the respective resonant frequencies at temperatures 25 °C and 85 °C.

3. Results and discussion

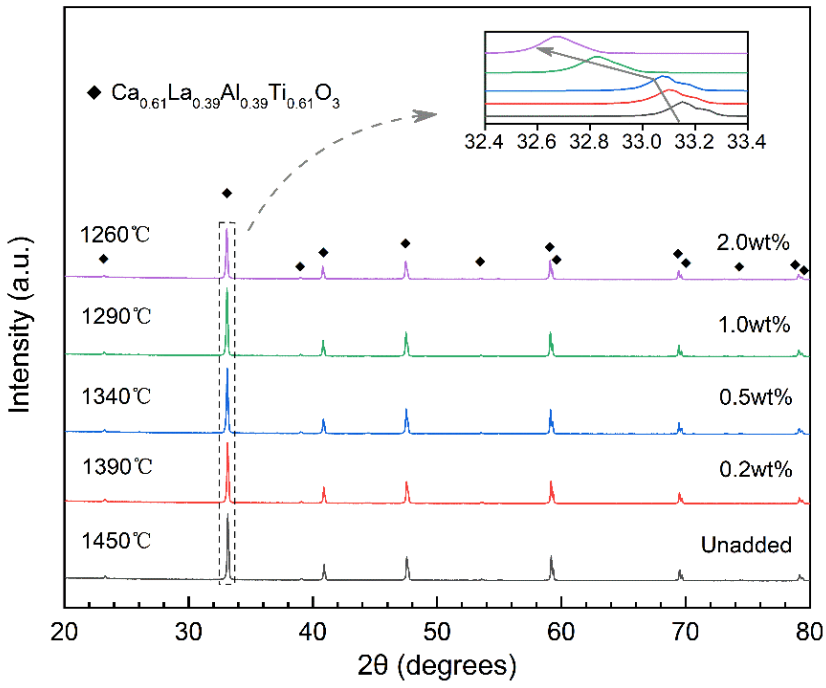

Fig. 1. X-ray diffraction patterns of $0.61CaTiO_3$-$0.39LaAlO_3$ ceramics with 0-2.0 wt% CaV_2O_6 sintered at 1260–1450 ℃ for 4 h.

Table 1. Polarizability, electronegativity and radius of the ions contained in $0.61CaTiO_3$-$0.39LaAlO_3$ ceramics and CaV_2O_6, as well as the electronegativity criterion (ΔS) and radius limit percentage (ΔR) based on V^{5+}.

Ion	Polarizability (Å^3)	Electronegativity	Radius (Å)	ΔS	ΔR (%)
Ca^{2+}	3.16	1.0	1.000	0.6	83.3
Ti^{4+}	2.93	1.5	0.605	0.1	13.0
La^{3+}	6.07	1.1	1.032	0.5	96.3
Al^{3+}	0.79	1.5	0.535	0.1	1.9
V^{5+}	2.92	1.6	0.540	-	-
O^{2-}	2.01	3.5	1.420	-	-

For $0.61CaTiO_3$-$0.39LaAlO_3$ ceramics, the addition of CaV_2O_6 prominently reduced the sintering temperature. At additive amounts of 0.2 wt%, 0.5 wt%, 1.0 wt% and 2.0 wt%, the optimum sintering temperatures were effectively decreased to 1390 ℃, 1340 ℃, 1290 ℃ and 1260 ℃, respectively. Fig. 1 presents the XRD patterns of CTLA ceramics with 0−2.0 wt% CaV_2O_6 sintered at 1260–1450 ℃ for 4 h. The $Ca_{0.61}La_{0.39}Al_{0.39}Ti_{0.61}O_3$ phase (PDF #52-1773) was obtained from all samples at all additive amounts and sintering temperatures, and there was no any secondary phase could be observed. This indicates the formation of a pure-phase solid solution. Table 1 lists the electronegativities and radii of the ions in CTLA and CaV_2O_6, as well as their electronegativity criterions (ΔS) and radius limit percentages (ΔR) based on V^{5+} [26, 27]. As shown in the table, the radius limit percentage (ΔR < 15%) and the electronegativity criterion (ΔS < 0.1) of V^{5+} in CaV_2O_6 versus Ti^{4+} and Al^{3+} in CTLA satisfied the conditions of ion substitution. And this led to the forming of the solid solution [24, 25].

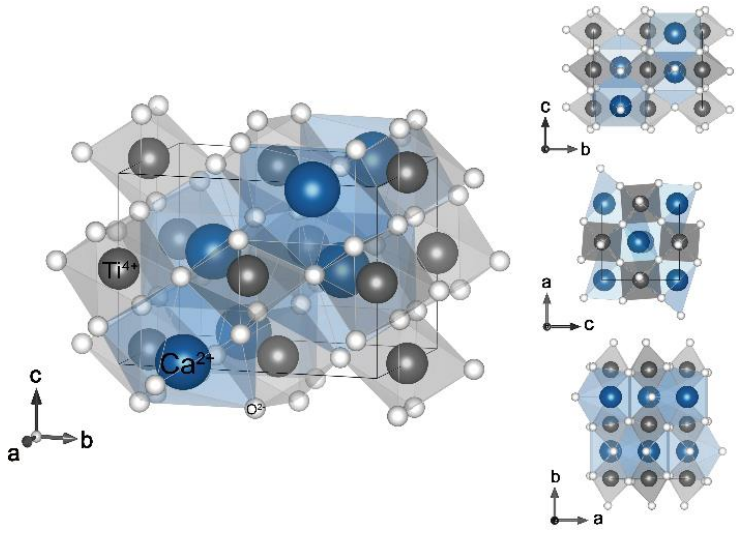

Fig. 2. Schematic crystal structure of $0.61CaTiO_3$-$0.39LaAlO_3$ ceramic.

It is worth noting that, as shown in the inset graph in Fig. 1, the strongest X-ray diffraction peaks gradually shifted toward the lower angles as the CaV_2O_6 content increased, which demonstrates the increase in cell volume [19]. As shown in the table 1, the ΔS of Al^{3+} and Ti^{4+} were approximately equal (1.5), but Al^{3+} had a much smaller ΔR (1.9) than Ti^{4+} (13.0), then the bigger V^{5+} preferentially and mainly replaced the smaller Al^{3+}. And this led to the increase of cell volume of the solid solution.

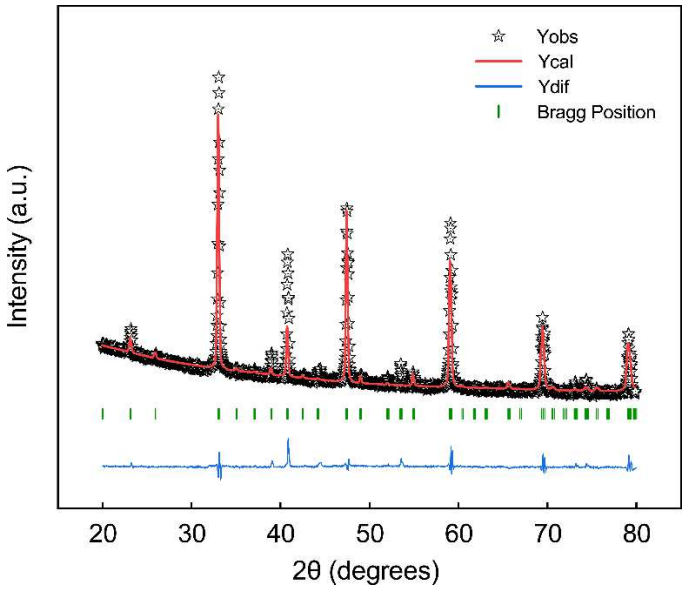

Fig. 3. Rietveld refinement patterns for $0.61CaTiO_3$-$0.39LaAlO_3$ ceramics with 1.0 wt% CaV_2O_6 sintered at 1290 ℃ for 4 h. Five-pointed stars are observed data. Red line is calculated data. Vertical lines present the Bragg position. Blue line is the difference between the observed and calculated data.

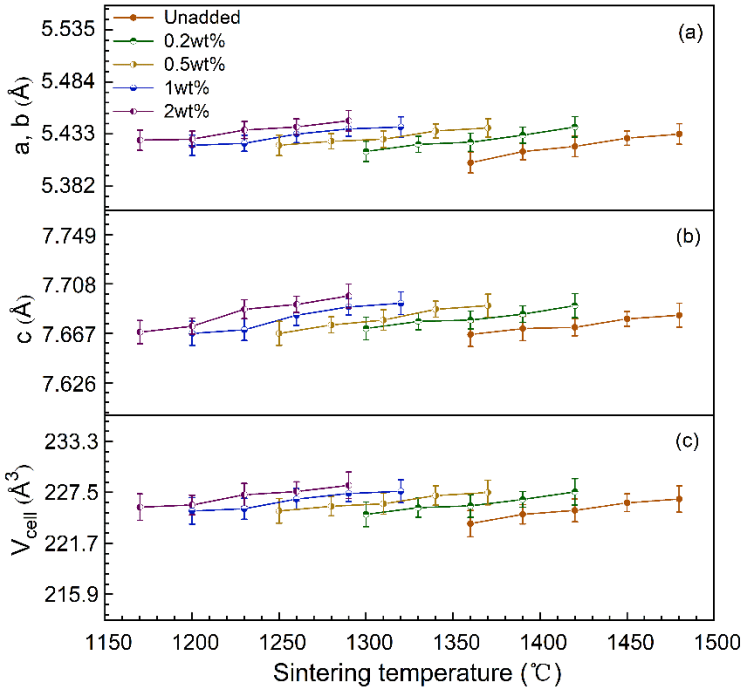

Fig. 4. Variation in lattice parameters of $0.61CaTiO_3$-$0.39LaAlO_3$ ceramics with 0−2.0 wt% CaV_2O_6 sintered at 1170−1480 ℃ for 4 h: (a) *a*, *b*; (b) *c*; (c) unit cell volume.

Table 2. Lattice parameters of 0.61$CaTiO_3$-0.39$LaAlO_3$ ceramics with 0−2.0 wt% CaV_2O_6 sintered at 1260−1450 °C for 4 h.

Composition	S. T. (°C)	Lattice parameters (Å)		β (°)	Vol (Å^3)	Discrepancy factors		
		a, *b*	*c*			R_p (%)	R_{wp} (%)	χ^2
Undoped	1450	5.429	7.679	90	226.33	4.15	3.56	3.124
0.2 wt%	1390	5.432	7.683	90	226.70	4.83	3.71	2.841
0.5 wt%	1340	5.436	7.687	90	227.15	4.32	3.89	3.264
1.0 wt%	1290	5.438	7.689	90	227.38	4.23	3.12	2.935
2.0 wt%	1260	5.440	7.691	90	227.60	4.76	3.45	3.451

0.61$CaTiO_3$-0.39$LaAlO_3$ ceramics have a cubic structure in space group *Pcmn*(62) with *Z* = 4; the schematic crystal structure is shown in Fig. 2. As depicted in Fig. 3, through the Rietveld refinement of the CTLA ceramics with 1.0 wt% CaV_2O_6 sintered at 1290 °C for 4 h, corresponding lattice parameters were obtained. Similarly, the lattice parameters of CTLA ceramics at all additive amounts and sintering temperatures were obtained. The results are listed in Table 2 and their variation trends are depicted in Fig. 4. It can be seen that the cell volume increased stepwise with the augment of CaV_2O_6, which conforms to the shifts in the strongest X-ray diffraction peaks.

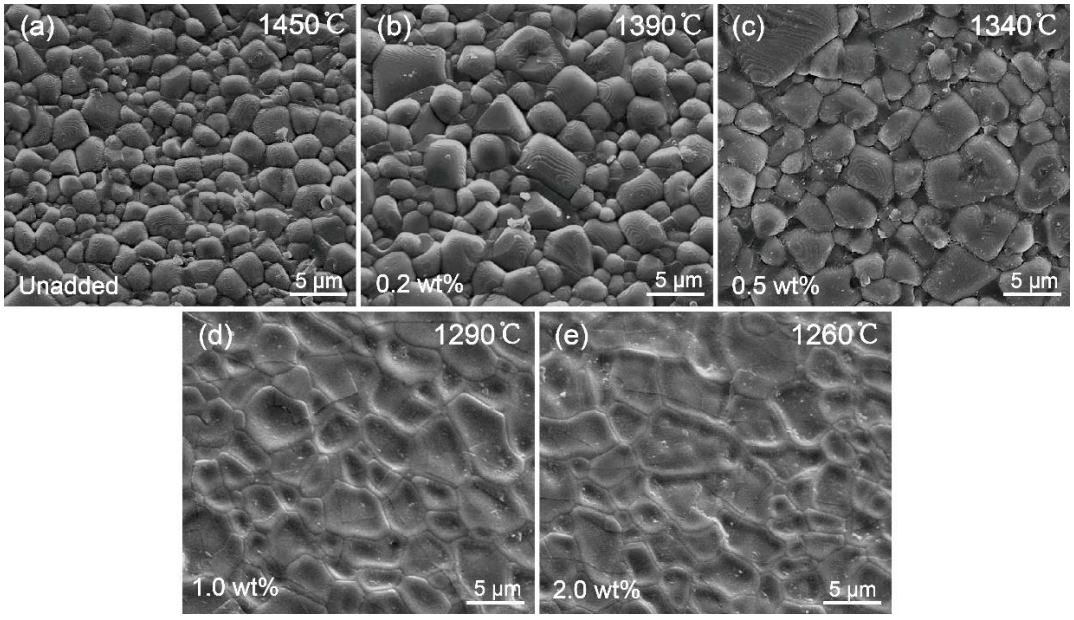

Fig. 5. SEM images of 0.61$CaTiO_3$-0.39$LaAlO_3$ ceramics with 0−2.0 wt% CaV_2O_6 sintered at 1260−1450 °C for 4 h: (a) unadded, (b) 0.2 wt%, (c) 0.5 wt%, (d) 1.0 wt%, (e) 2.0 wt%.

Fig. 5 shows the SEM images of the 0.61$CaTiO_3$-0.39$LaAlO_3$ ceramics with 0–2.0 wt% CaV_2O_6 sintered at 1260–1450 °C for 4 h. At each additive amount, the grains presented similar sizes and shapes with homogeneous distributions, which was in line with the morphological

characteristics of general single-phase ceramics. For the CaV_2O_6-free CTLA ceramics, a high-compactness and low-porosity microstructure with grain size about 3.0 μm was observed (Fig. 5 (a)). At the CaV_2O_6 content of 0.2 wt%, the grains grew bigger and fuller with sizes of 3.0–5.0 μm, and the grain boundaries became distinct (Fig. 5 (b)). With 0.5 wt% CaV_2O_6 added, continuously-grown grains began to flatten with sizes of about 4.0–6.0 μm, the compactness increased, and the number of pores decreased (Fig. 5 (c)). When the CaV_2O_6 content increased to 1.0 wt%, the grains further grew bigger and exhibited more flat morphology with sizes of 5.0–7.0 μm, and the grain boundaries became significantly clearer. An excellent microstructure with relatively high density and low porosity was achieved (Fig. 5 (d)). However, as the CaV_2O_6 content continued to increase, grain growth stopped and some of the grain boundaries became fuzzy, which indicates a slight deterioration in morphology (Fig. 5 (e)).

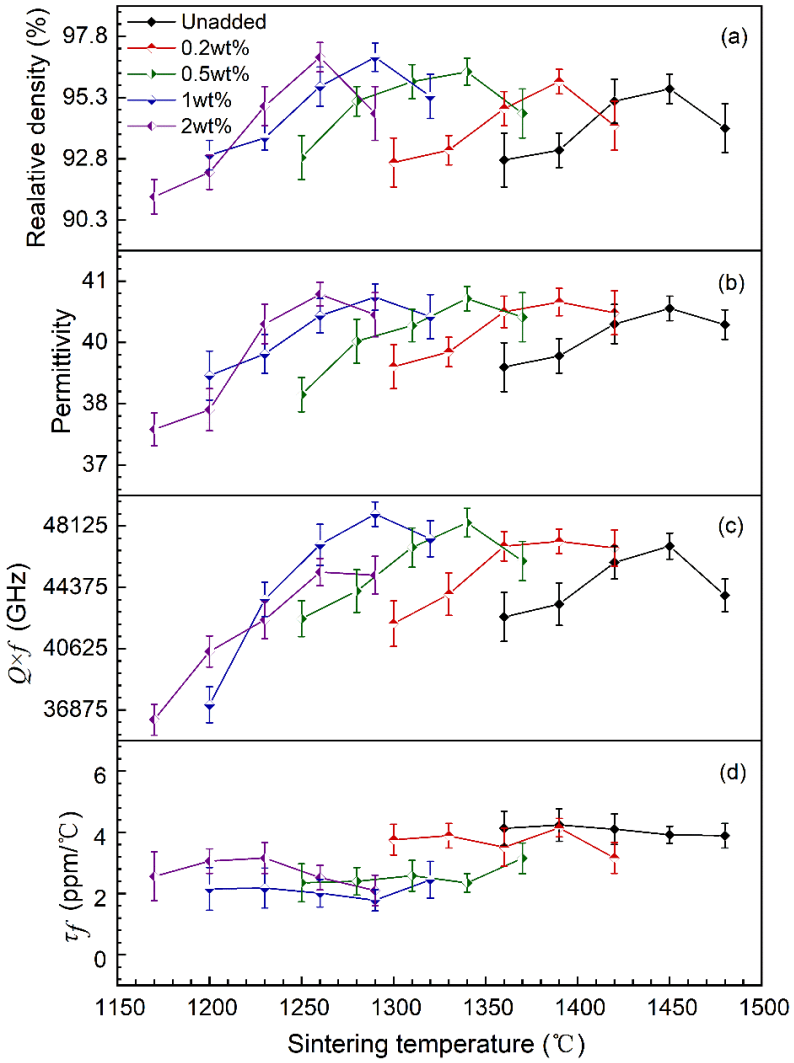

Fig. 6. Variations in (a) relative density, (b) ε_r, (c) $Q \times f$, and (d) τ_f in $0.61CaTiO_3$-$0.39LaAlO_3$ ceramics with 0–2.0 wt% CaV_2O_6 sintered at 1170–1480 °C for 4 h.

Fig. 6 presents the variations in relative density, ε_r, $Q\times f$ and τ_f of $0.61CaTiO_3$-$0.39LaAlO_3$ ceramics with 0–2.0 wt% CaV_2O_6 sintered at 1170–1480 ℃ for 4 h. The trend in relative density is shown in Fig. 6 (a); at a constant amount of additive, the relative density first increased and then decreased sintering temperature. The increasing stage is attributed to the continuous growth of grains and continuous decreases in porosity, while the decreasing stage is attributed to grain boudaries being obscured and the pores not being fully discharged at excessively high sintering temperatures. As the additive amount increased, the relative densities of CTLA ceramics obtained at their respective optimal sintering temperatures gradually increased, which indicates that CaV_2O_6 addition promotes the densification sintering of CTLA ceramics. The CTLA ceramic sintered at 1290 ℃ for 4 h with a CaV_2O_6 content of 1.0 wt% exhibited the highest relative density of 96.9%.

Fig. 6 (b) shows the variation in ε_r value of CTLA ceramics according to CaV_2O_6 addition amount and sintering temperature. At a given CaV_2O_6 content, the ε_r increased first and then decreased with increasing sintering temperature. With the increasing of additive amount in 0−2.0 wt%, the dielectric constant of the CTLA ceramics obtained at respective optimal sintering temperatures increase continuously and slightly. The dielectric constant exhibited the same trend as relative density. This phenomenon is attributed to the permittivity of pure-phase ceramics being positively correlated with relative density at extrinsic level [28]. In addition, at intrinsic level, molecular polarizability is also the primary factor affecting permittivity [29]. Molecular polarizability of the CTLA solid solutions can be calculated by Shannon's additive rule [30-32]:

$$\alpha = (0.61 + x)\alpha(Ca^{2+}) + 0.61\alpha(Ti^{4+}) + 0.39\alpha(La^{3+}) + 0.39\alpha(Al^{3+}) + 2x\alpha(V^{5+}) + (3 + 6x)\alpha(O^{2-}) \quad (0 < x < 0.014) \tag{6}$$

Where the x is molar amount of CaV_2O_6. And according to the ion polarizabilities listed in Table 1 [30], the calculation results show that the molecular polarizability increased with increasing CaV_2O_6 content, then the macroscopic performance is the augmentation of permittivity. The maximum permittivity of 40.6 occurred in the CTLA ceramic with 1.0 wt% CaV_2O_6 sintered at 1290 ℃ for 4 h .

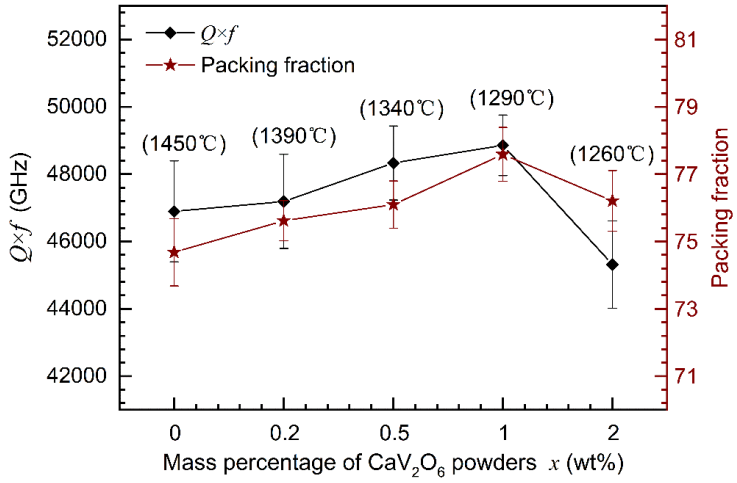

Fig. 7. Variations in the $Q\times f$ values and packing fractions of $0.61CaTiO_3$-$0.39LaAlO_3$ ceramics with 0–2.0wt% CaV_2O_6 sintered at their optimum sintering temperatures for 4 h.

Fig. 6 (c) illustrates the $Q\times f$ trends of $0.61CaTiO_3$-$0.39LaAlO_3$ ceramics with 0–2.0 wt% CaV_2O_6 sintered at 1170–1480 ℃ for 4 h. Values of $Q\times f$ still showed trends consistent with relative density, which is ascribed to the fact that relative density is the pivotal extrinsic factor affecting $Q\times f$ [28]. At intrinsic level, there is a relationship between packing fraction and dielectric loss. The packing fraction was calculated as [33]:

$$packing\ \ fraction = \frac{\sum V_{atoms}}{V_{molar-volume}} \tag{7}$$

Where $\sum V_{atoms}$ is the sum of the volume of each atom, and $V_{molar-volume}$ is the molar volume. Fig. 7 shows the variations in $Q\times f$ and packing fraction of $0.61CaTiO_3$-$0.39LaAlO_3$ ceramics with 0–2.0 wt% CaV_2O_6 sintered at their respective optimal sintering temperatures for 4 h. At the CaV_2O_6 content of 1.0 wt%, the $Q\times f$ value of CTLA ceramics sintered at 1290 ℃ for 4 h reached the maximum 48,800 GHz.

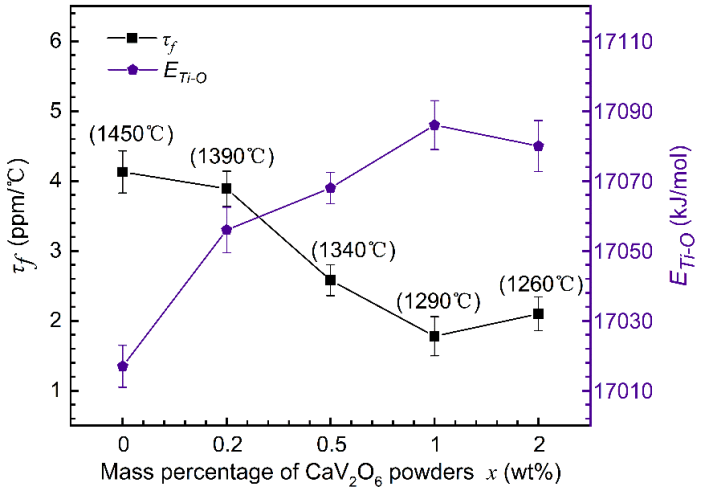

Fig. 8. Variations in τ_f and Ti-O bond energy of $0.61CaTiO_3$-$0.39LaAlO_3$ ceramics with 0–2.0 wt% CaV_2O_6 sintered at their optimum sintering temperatures for 4 h.

Fig. 6 (d) presents the variation in τ_f of 0.61$CaTiO_3$-0.39$LaAlO_3$ ceramics with 0–2.0 wt% CaV_2O_6 sintered at 1170–1480 °C for 4 h. With continuous increases in additive amount, the τ_f showed a trend of first decreasing and then increasing. At intrinsic level, the bond energy represents the energy required to break chemical bonds, which greatly determines the thermal stability and affects the τ_f value [34-36]. The bond energy is composed of complete ionic energy (E_i^u) and non-polar covalent energy (E_c^u), and is calculated as:

$$E = x_i E_i^u + x_c E_c^u \tag{8}$$

$$E_i = \frac{33200}{d} \tag{9}$$

$$E_c^u = \frac{(r_A + r_B)}{d}(E_A E_B)^{1/2} \tag{10}$$

Where d is the bond length, r_A and r_B are the covalent radii of ions A and B, and E_A and E_B are their homonuclear bond energies. The bond length and covalent radii in the CTLA lattice were obtained by refinement in GSAS software [37], and the homonuclear bond energies were taken from the literature [34]. Fig. 8 shows the variations in the τ_f and Ti-O bond energy of 0.61$CaTiO_3$-0.39$LaAlO_3$ ceramics with 0–2.0 wt% CaV_2O_6 sintered at their optimum sintering temperatures for 4 h. With increases in CaV_2O_6 addition, the Ti-O bond energy gradually increased, which meant that the thermal stability of the chemical bonds increased, causing τ_f to approach zero in macroscopic performance. With a CaV_2O_6 additive amount of 1.0 wt%, the τ_f value of CTLA ceramics sintered at 1290 °C reached a perfect value of 0.78 ppm/°C.

4. Conclusions

CaV_2O_6 is an extremely effective sintering aid for 0.61$CaTiO_3$-0.39$LaAlO_3$ ceramics. When the CaV_2O_6 was introduced to CTLA ceramics, additions of 0–2.0 wt% CaV_2O_6 could be dissolved into CTLA lattice to form a pure-phase solid solution. Meanwhile, the bigger V^{5+} replaced the smaller Al^{3+} and led to the increase of cell volume of the solid solution, the polarization per cell volume increased and led to the improvement of permittivity, the packing fraction improved and led to the significant increase of $Q\times f$ value, the Ti-O bond energy strengthened and led to the approach 0 of τ_f value. For the CTLA ceramics, addition of 1.0 wt% CaV_2O_6 could high-effectively lower the sintering temperature from 1450 °C to 1290 °C and favorably enhance the performance with ε_r = 40.6, $Q\times f$ = 48,800 GHz (at 4.5 GHz), and τ_f = 0.78 ppm/°C. This provides a new way of low firing and property modification for high-temperature MWDCs.

Acknowledgments

This work was supported by the National Science Foundation of China (Grant Nos. 11902316, 11972333 and 51902300), the National Science Foundation of Zhejiang Province (Grant Nos. LZ19A020001 and LQ19F010005) and the Open Foundation of the State Key Laboratory of Electronic Thin Films and Integrated Devices (KFJJ202003). Han Yang also acknowledge the start-up fund of China Jiliang University (Grant No. 190743).

References

[1] Reaney IM, Iddles D. Microwave dielectric ceramics for resonators and filters in mobile phone networks. *J Am Ceram Soc* 2006, **89**: 2063–2072.

[2] Wang S, Luo WJ, Li LX, *et al*. Improved tri-layer microwave dielectric ceramic for 5G applications. *J Eur Ceram Soc* 2021, **41**: 418–423.

[3] Su CH, Wang YS, Huang CL. Characterization and microwave dielectric properties of Mg_2YVO_6 ceramic. *J Alloy Compd* 2015, **641**: 93–98.

[4] Xu NX, Zhou JH, Yang H, *et al*. Structural evolution and microwave dielectric properties of MgO–LiF co-doped Li_2TiO_3 ceramics for LTCC applications. *Ceram Int* 2014, **40**: 15191–15198.

[5] Lv XS, Li LX, Sun H, *ea al*. Microwave dielectric properties of novel temperature stable high Q $MgZr_{1+x}Nb_2O_{8+2x}$ ceramics. *Ceram Int* 2015, **41**: 15287–15291.

[6] Pang LX, Liu WG, Zhou D, *et al*. Novel glass-free low-temperature fired microwave dielectric ceramics: $Bi(Ga_{1/3}Mo_{2/3})O_4$. *Ceram Int* 2016, **42**: 4574–4577.

[7] Kipkoech ER, Azough F, Freer R, *et al*. Structural study of $Ca_{0.7}Nd_{0.3}Ti_{0.7}Al_{0.3}O_3$ dielectric ceramics using synchrotron X-ray diffraction. *J Eur Ceram Soc* 2003, **23**: 2677–2682.

[8] Chen YB. Structural and dielectric properties of $La(Mg_{1/2}Ti_{1/2})O_3$–$Ca_{0.6}La_{0.8/3}TiO_3$-doped CuO. *J Alloy Compd* 2009, **480**: 820–823.

[9] Lei SH, Fan HQ, Chen WN, *et al*. Structure, Microwave Dielectric Properties, and Novel Low-Temperature Sintering of $xSrTiO_3$-(1-x)$LaAlO_3$ Ceramics with LTCC Application. *J Am Ceram Soc* 2017, **100**: 235–246.

[10] Chen AN, Wu JM, Cheng LJ, *et al*. Enhanced densification and dielectric properties of $CaTiO_3$-$0.3NdAlO_3$ ceramics fabricated by direct coagulation casting. *J Eur Ceram Soc* 2020, **40**: 1174–1180.

[11] Hameed I, Liu XQ, Li L, *et al*. Structure evolution and improved microwave dielectric characteristics in $CaTi_{1-x}(Al_{0.5}Nb_{0.5})_xO_3$ ceramics. *J Alloy Compd* 2020, **845**: 155435.

[12] Moon JH, Jang HM, Park HS, *et al*. Sintering behavior and microwave dielectric properties of (Ca, La)(Ti, Al)O_3 Ceramics. *Jpn J Appl Phys* 1999, **38**: 6821.

[13] Suvorov D, Valant M, Jančar B, *et al*. $CaTiO_3$-based ceramics: microstructural development and dielectric properties. *Acta Chim Slov* 2001, **48**: 87–99.

[14] Jiang J, Fang DH, Lu C, *et al*. Solid-state reaction mechanism and microwave dielectric properties of $CaTiO_3$–$LaAlO_3$ ceramics. *J Alloy Compd* 2015, **638**: 443–447.

[15] Tang B, Fang ZX, Li H, *et al*. Microwave dielectric properties of H_3BO_3-doped $Ca_{0.61}La_{0.39}Al_{0.39}Ti_{0.61}O_3$ ceramics. *J Mater Sci-Mater Electron* 2014, **26**: 300–306.

[16] Weng MH, Liauh CT, Lin SM, *et al*. Sintering behaviors, microstructure, and microwave dielectric properties of $CaTiO_3$–$LaAlO_3$ ceramics using CuO/B_2O_3 additions. *Materials* 2019, **12**: 4187.

[17] Xi J, Chen GH, Liu F, *et al*. Synthesis, microstructure and characterization of ultra-low permittivity CuO–ZnO–B_2O_3–Li_2O glass/Al_2O_3 composites for ULTCC application. *Ceram Int* 2019, **45**: 24431–24436.

[18] Zhuk NA, Shugurov SM, Krzhizhanovskaya MG, *et al*. The effect of CuO on the microstructure, spectral characteristics, thermal and electrical properties of $BiNbO_4$ ceramics. *J Alloy Compd* 2020, **822**: 153619.

[19] Pirvaram A, Taheri-Nassaj E, Taghipour-Armaki H, *et al*. Study on structure, microstructure and microwave dielectric characteristics of CaV_2O_6 and $(Ca_{0.95}M_{0.05})V_2O_6$ (M=Zn, Ba) ceramics. *J Am Ceram Soc* 2019, **102**: 5213–5222.

[20] Yao GG, Pei CJ, Xu JG, *et al*. Microwave dielectric properties of CaV_2O_6 ceramics with low dielectric loss. *J Mater Sci-Mater Electron* 2015, **26**: 7719–7722.

[21] Xiang HC, Li CC, Yin CZ, *et al*. A reduced sintering temperature and improvement in the microwave dielectric properties of $Li_2Mg_3TiO_6$ through Ge substitution. *Ceram Int* 2018, **44**: 5817–5821.

[22] Yang H, Tang B, Fang ZX, *et al*. A new low-firing and high-Q microwave dielectric ceramic $Li_9Zr_3NbO_{13}$. *J Am Ceram Soc* 2018, **101**: 2202–2207.

[23] Yao GG, Ren ZY, Liu P. Effect of Ca substitution on microwave dielectric properties of BaV_2O_6 ceramics. *J Electroceram* 2018, **40**: 144–149.

[24] Kumar A, Varshney D. Crystal structure refinement of $Bi_{1-x}Nd_xFeO_3$ multiferroic by the Rietveld method. *Ceram Int* 2012, **38**: 3935–3942.

[25] Wang G, Zhang DN, Li J, *et al*. Crystal structure, bond energy, Raman spectra, and microwave dielectric properties of Ti-doped $Li_3Mg_2NbO_6$ ceramics. *J Am Ceram Soc* 2020, **103**: 4321–4332.

[26] Karimi S, Reaney IM, Levin I, *et al*. Nd-doped $BiFeO_3$ ceramics with antipolar order. *Appl Phys Lett* 2009, **94**: 112903.

[27] Shannon RD. Revised effective ionic radii and systematic studies of interatomic distances in halides and chalcogenides. *Acta Chim Slov* 1976, **32**: 751–767.

[28] Zheng JJ, Xu HZ, Yang YK, *et al*. Sintering behavior and microwave dielectric properties of LiF-doped $Li_2Mg_3Ti_{0.95}(Mg_{1/3}Ta_{2/3})_{0.05}O_6$ ceramics for LTCC applications. *J Electron Mater* 2019, **49**: 773–779.

[29] Zhang P, Hao MM, Mao XR, *et al*. Effects of W^{6+} substitution on crystal structure and microwave dielectric properties of $Li_3Mg_2NbO_6$ ceramics. *Ceram Int* 2020, **46**: 21336–21342.

[30] Zhang P, Hao MM, Xiao M. Microwave dielectric properties of $Li_3Mg_2NbO_6$-based ceramics with $(M_xW_{1-x})^{5+}$ ($M = Li^+$, Mg^{2+}, Al^{3+}, Ti^{4+}) substitutions at Nb^{5+} sites. *J Alloy Compd* 2021, **853**: 157386.

[31] Templeton A, Wang XR, Penn SJ, *et al.* Microwave dielectric loss of titanium oxide. *J Am Ceram Soc* 2010, **83**: 95–100.

[32] Zhang P, Sun KX, Xiao M, *et al*. Crystal structure, densification, and microwave dielectric properties of $Li_3Mg_2(Nb_{(1-x)}Mo_x)O_{6+x/2}$ ($0 \leqslant x \leqslant 0.08$) ceramics. *J Am Ceram Soc* 2019, **102**: 4127–4135.

[33] Kim ES, Chun BS, Freer R, *et al*. Effects of packing fraction and bond valence on microwave dielectric properties of $A^{2+}B^{6+}O_4$ (A^{2+}: Ca, Pb, Ba; B^{6+}: Mo, W) ceramics. *J Eur Ceram Soc* 2010, **30**: 1731–1736.

[34] Sanderson RT. Bond energies, *J Inorg Nucl Chem* 1966, **28**: 1553–1565.

[35] Shi L, Peng R, Zhang HW, *et al*. Effects of magnesium–tungsten co-substitution on crystal structure and microwave dielectric properties of $CaTi_{1-x}(Mg_{1/2}W_{1/2})_xO_3$ ceramics. *Ceram Int* 2020, **47**: 3354–3360.

[36] Xiao M, Zhang P, Lou J, *et al*. Combined synthesis methods for producing $LaNbO_4$ ceramics and

investigation of microwave dielectric properties based on complex chemical bond theory. *J Alloy Compd* 2020, **812**: 152154.

[37] Toby BH, Dreele RBV. GSAS-II: the genesis of a modern open-source all purpose crystallography software package. *J Appl Crystallogr* 2013, **46**: 544–549.

Figures

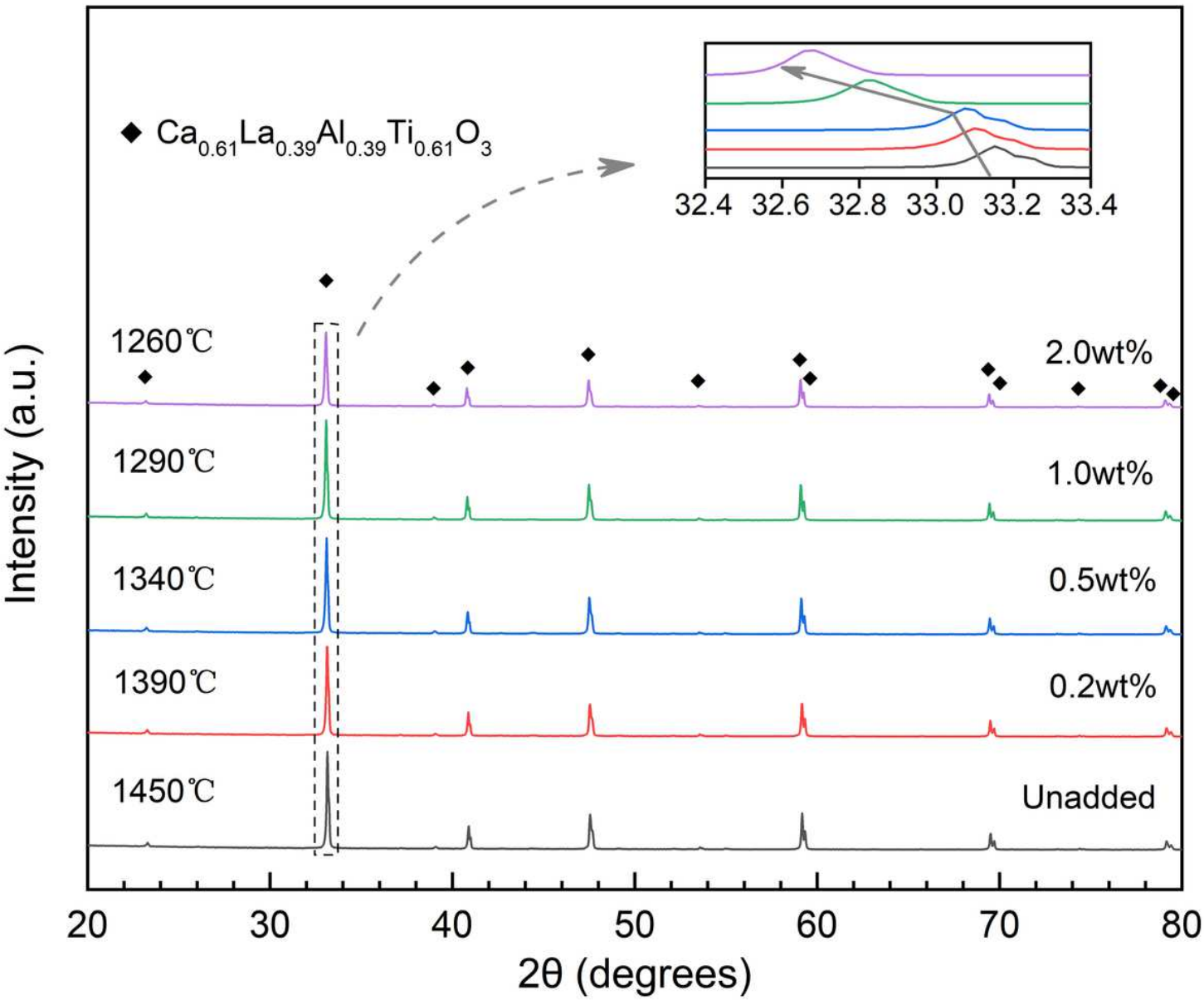

Figure 1

X-ray diffraction patterns of 0.61CaTiO3-0.39LaAlO3 ceramics with 0-2.0 wt% CaV2O6 sintered at 1260–1450 □ for 4 h.

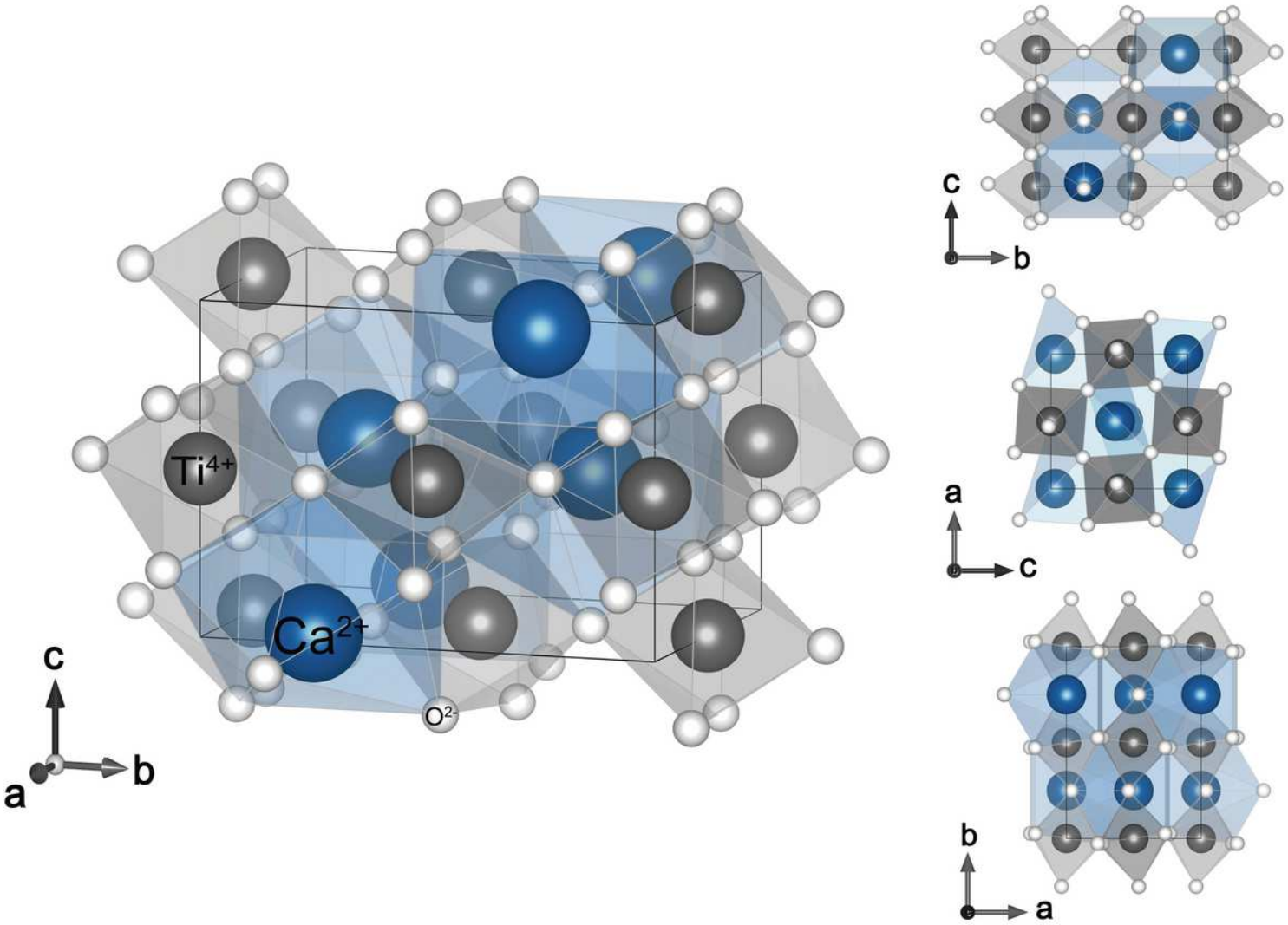

Figure 2

Schematic crystal structure of 0.61CaTiO3-0.39LaAlO3 ceramic

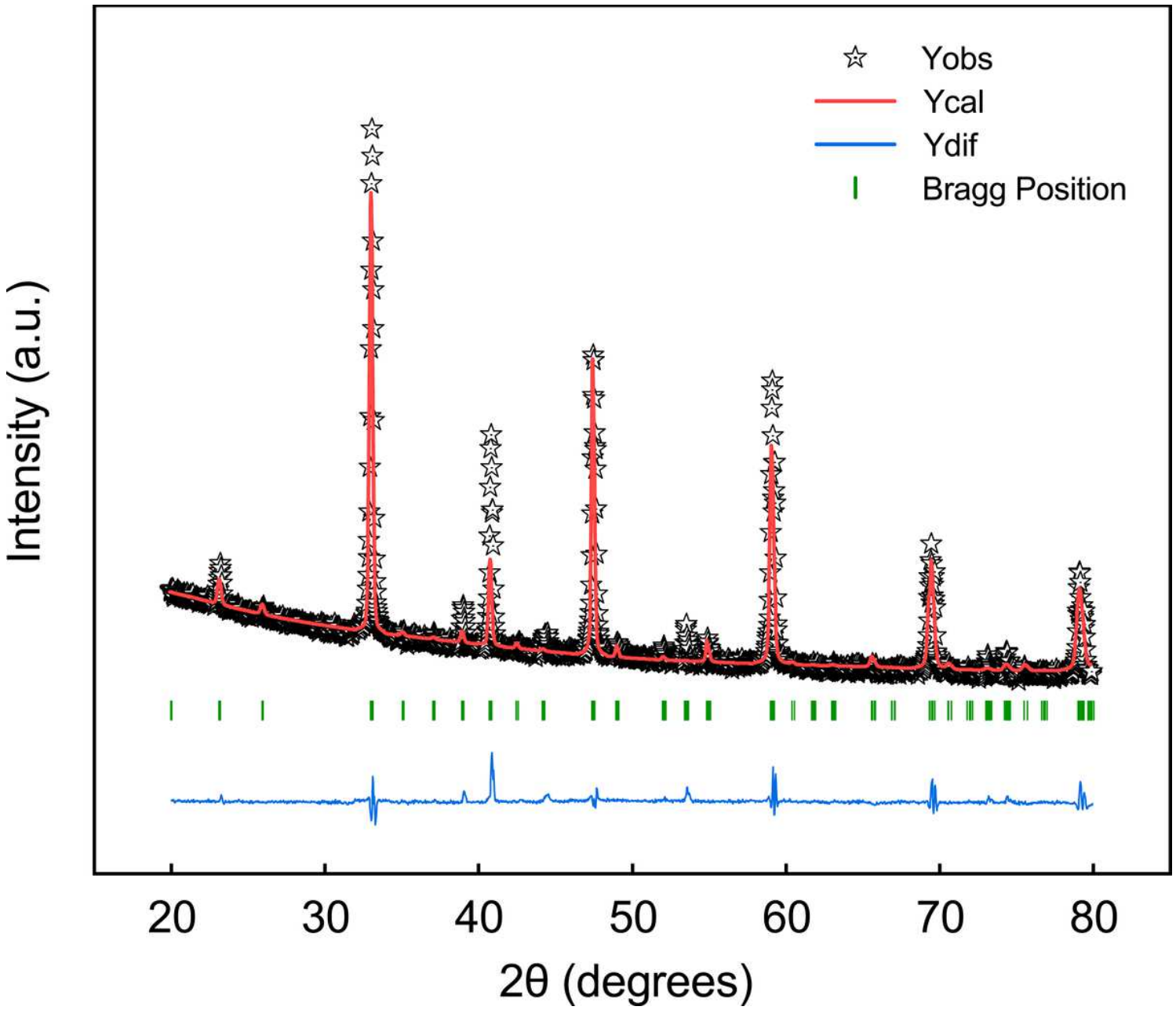

Figure 3

Rietveld refinement patterns for 0.61CaTiO3-0.39LaAlO3 ceramics with 1.0 wt% CaV2O6 sintered at 1290 □ for 4 h. Five-pointed stars are observed data. Red line is calculated data. Vertical lines present the Bragg position. Blue line is the difference between the observed and calculated data.

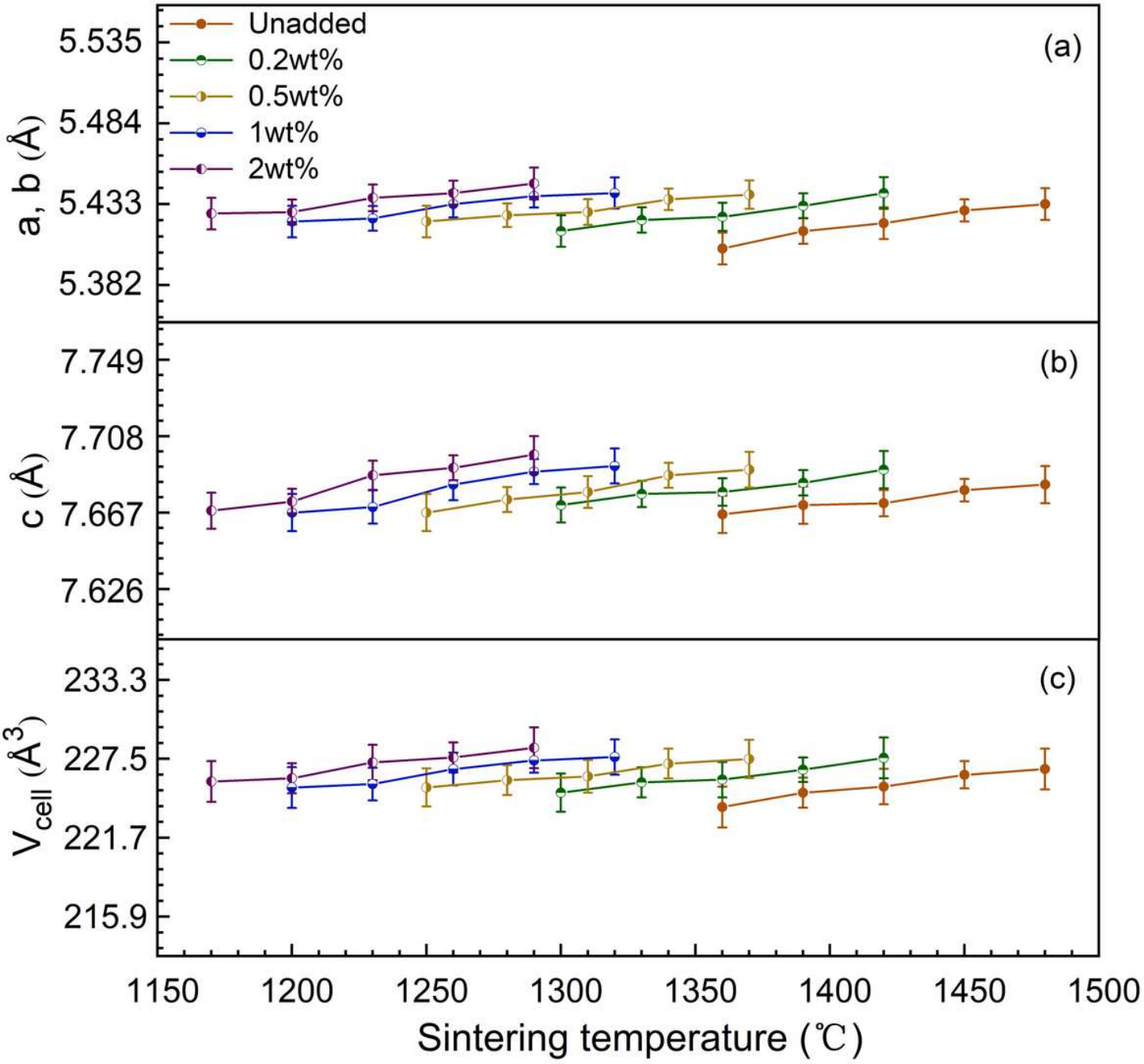

Figure 4

Variation in lattice parameters of 0.61CaTiO3-0.39LaAlO3 ceramics with 0–2.0 wt% CaV2O6 sintered at 1170–1480 ℃ for 4 h: (a) a, b; (b) c; (c) unit cell volume.

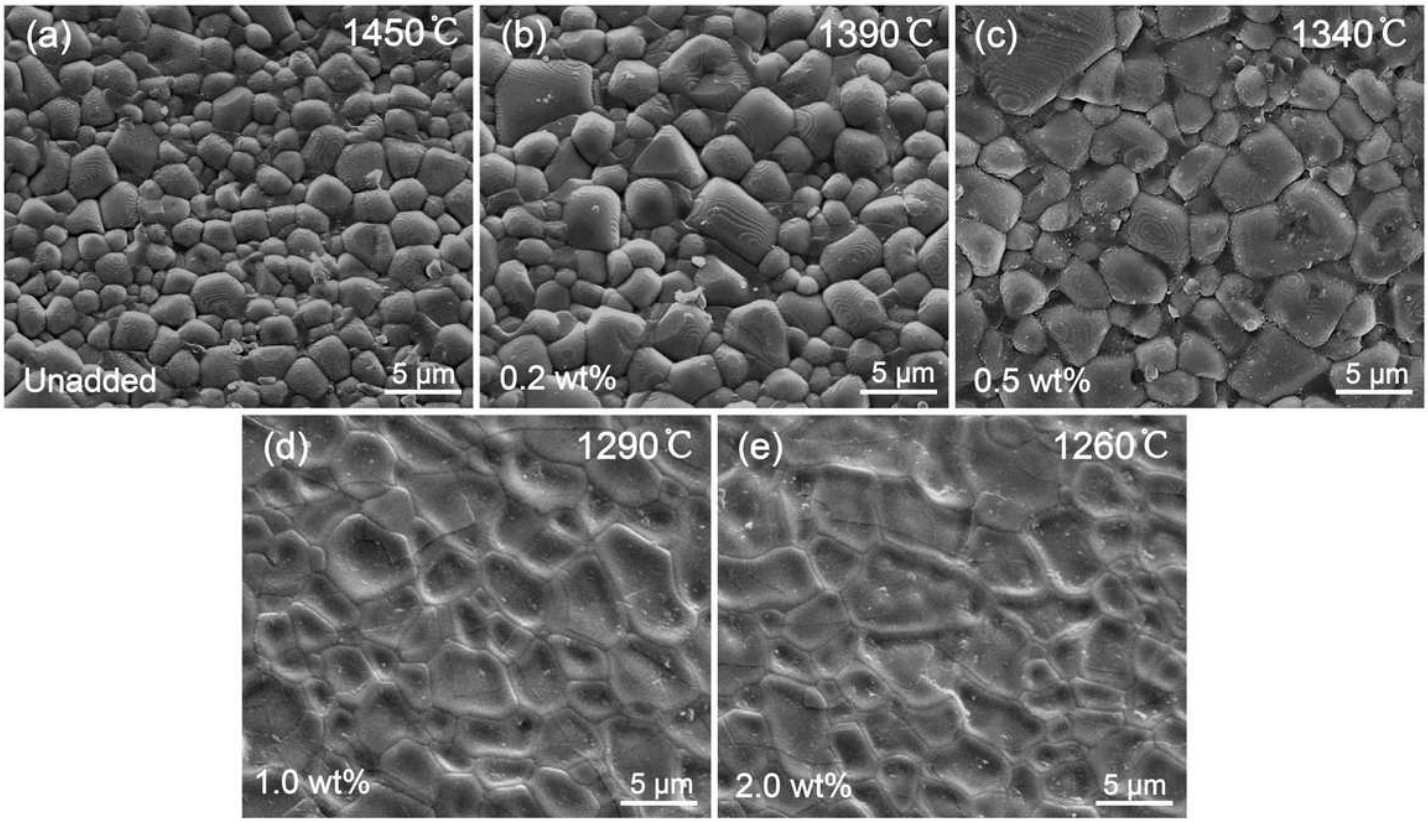

Figure 5

SEM images of 0.61CaTiO3-0.39LaAlO3 ceramics with 0–2.0 wt% CaV2O6 sintered at 1260–1450 □ for 4 h: (a) unadded, (b) 0.2 wt%, (c) 0.5 wt%, (d) 1.0 wt%, (e) 2.0 wt%.

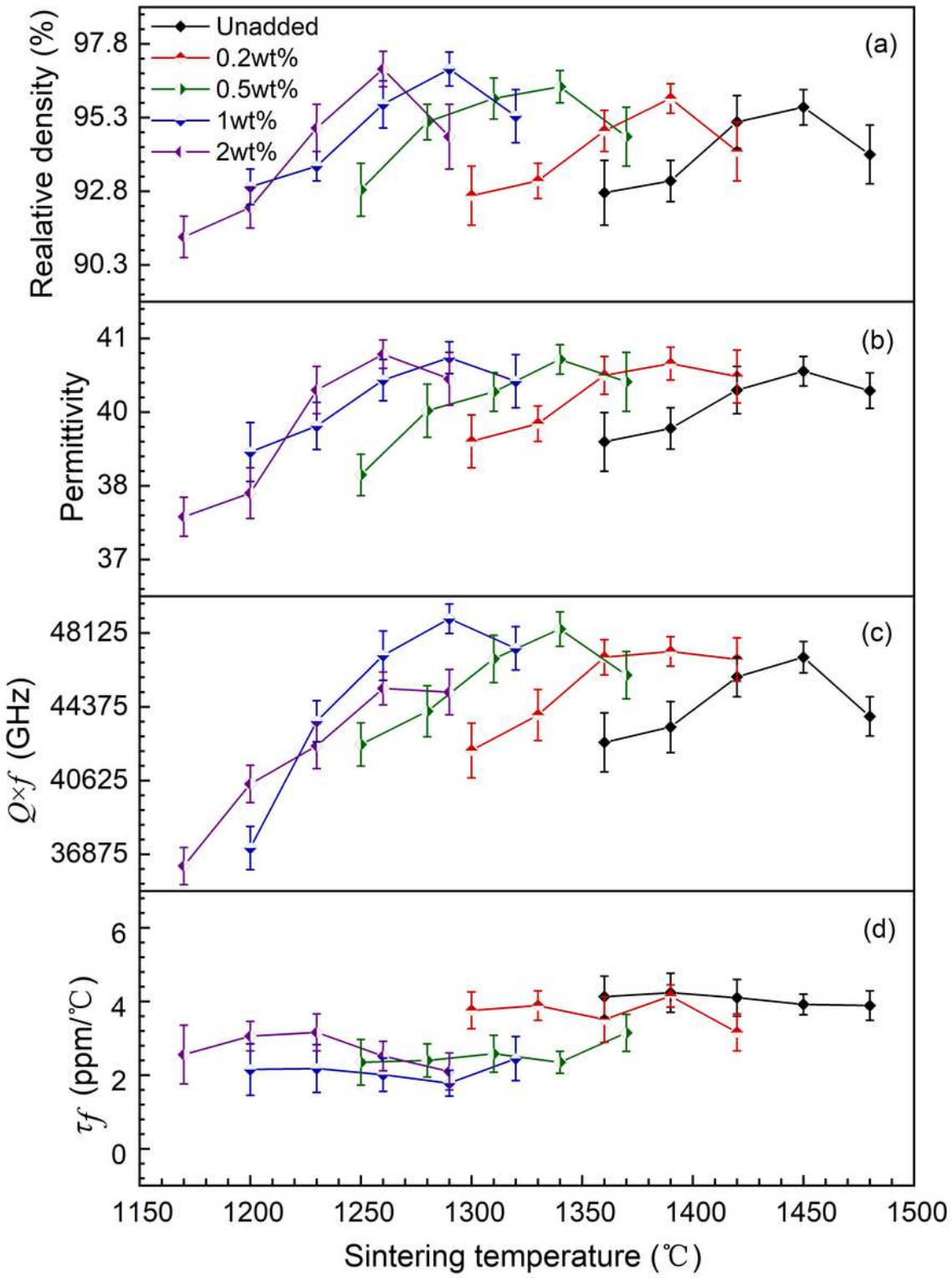

Figure 6

Variations in (a) relative density, (b) εr, (c) Q × f, and (d) τf in 0.61CaTiO3-0.39LaAlO3 ceramics with 0–2.0 wt% CaV2O6 sintered at 1170–1480 ℃ for 4 h.

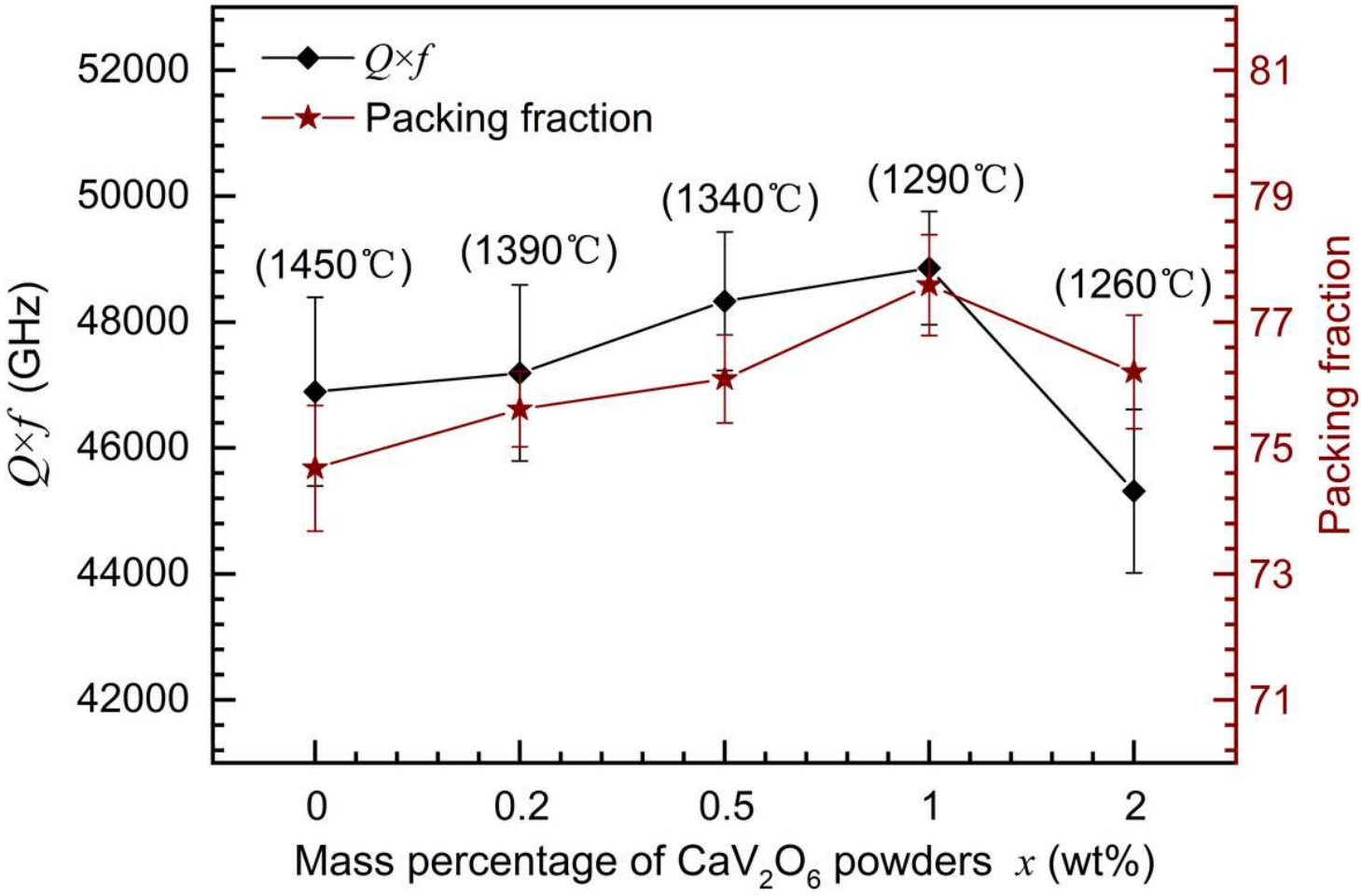

Figure 7

Variations in the Q×f values and packing fractions of 0.61CaTiO3-0.39LaAlO3 ceramics with 0–2.0wt% CaV2O6 sintered at their optimum sintering temperatures for 4 h.

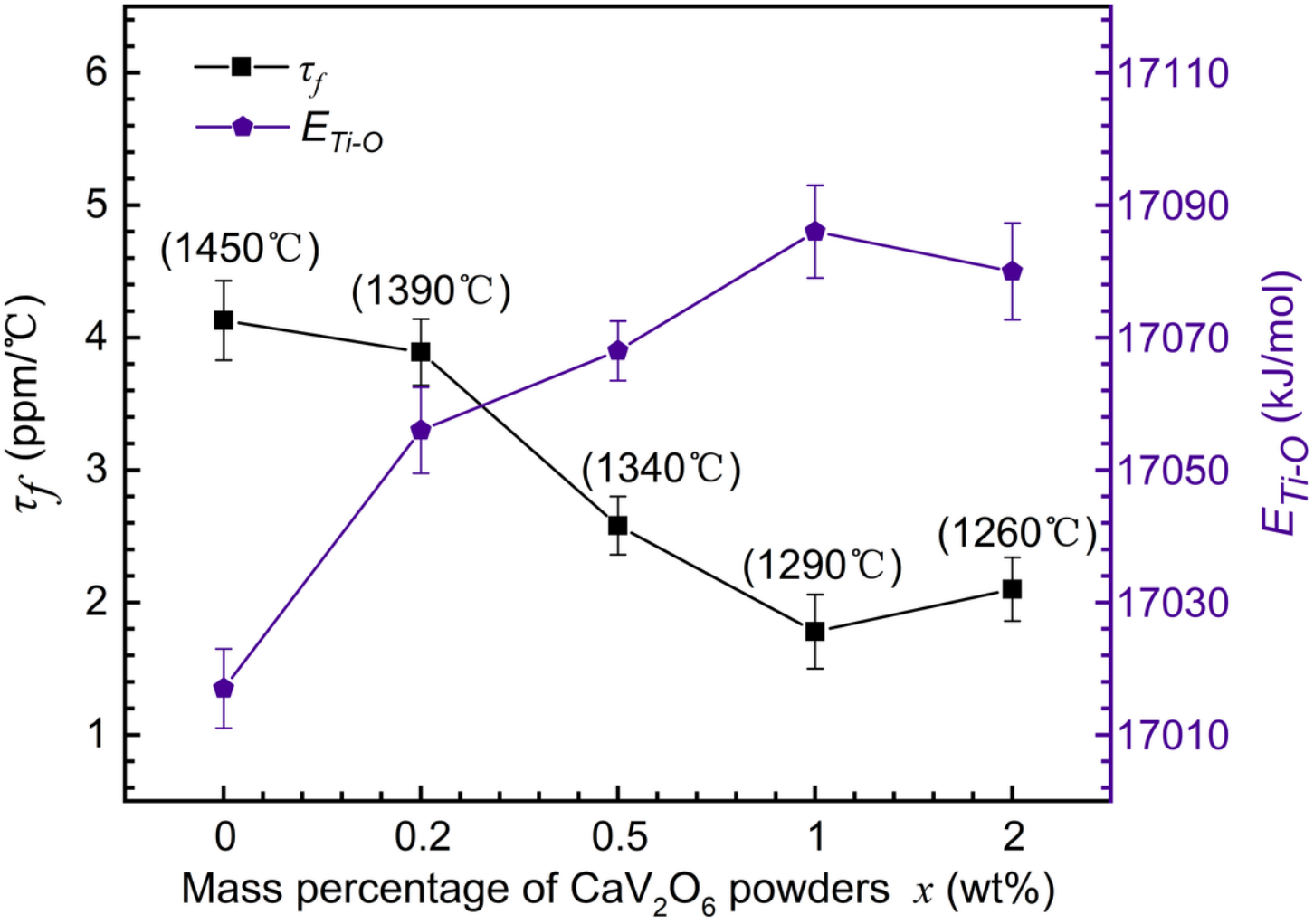

Figure 8

Variations in τf and Ti-O bond energy of 0.61CaTiO3-0.39LaAlO3 ceramics with 0–2.0 wt% CaV2O6 sintered at their optimum sintering temperatures for 4 h.

Supplementary Files

This is a list of supplementary files associated with this preprint. Click to download.

- DeclarationofInterestStatement.docx